Coherence Addressing of Quasi-Distributed Absorption Sensors by the FMCW Method

Miha Završnik and George Stewart

***Abstract*—We report a new addressing mechanism for quasi-distributed absorption sensors based on the frequency modulated continuous wave (FMCW) method. The sensor units consist of open-path microoptic cells constructed from gradient index (GRIN) lenses, each of differing lengths. Coherence addressing of the cells using FMCW is achieved by the interferometric mixing of two signals originating from each cell (from the glass/air interfaces). The time delay between the two reflections, along with the linear frequency ramp of the source, gives rise to beat frequencies in the mixed output which are different for each cell. The connecting fiber length between two successive sensor cells is chosen to be much greater than the coherence length of the source so that the reflections from different cells do not interfere. The interference patterns of all sensor cells add up at the detector whereby each individual sensing cell is identified by its power spectrum in the frequency domain. We show theoretically and experimentally how individual cells can be addressed and the measured signals obtained by suitable choice of cell length, proper modulation of the source and appropriate signal processing.**

***Index Terms*—Absorption sensors, distributed fiber sensors, frequency-modulated continuous-wave (FMCW) method.**

I. Introduction

ADVANCED technologies are becoming more and more critical to chemical and environmental sensing, efficient pollution prevention and cost effective industrial process control. The field of fiber optic sensors has expanded rapidly in the last decade and fiber based sensors have been developed for the measurement of a variety of physical and chemical parameters including chemical concentration and characterization of chemical species present in mixtures. Ideally these sensor systems would be capable of making distributed measurements of any given analyte or gas.

With the development of optical fiber interferometric sensors, interest in multiplexing several sensors in a system has greatly increased. Fiber sensors offer unique capabilities when configured in a distributed nature, or arranged in multiplexing networks. Such systems allow sensing at a large number of points by combining fiber-sensing methodologies with fiber telemetry. The primary emphasis in designing a sensor array is the method of separating individual sensor signals. A number of different multiplexing topologies have been devised and tested in recent years including time-division multiplexing (TDM), wavelength division multiplexing (WDM), coherence multiplexing [1] and frequency division multiplexing [2]. As an alternative to optical time-domain reflectometry [4], frequency-modulated continuous- wave reflectometry has been introduced, and investigations on multiplexing optical fiber sensors using a frequency-modulated source [5] have been accomplished.

In this paper, we present a combination of coherence addressing and the frequency modulated continuous wave method (FMCW) to distinguish between different open-path microoptic sensing units arranged in series. Coherence addressing of the cells using FMCW is achieved by the interferometric mixing of two signals originating from each cell (from the glass/air interfaces). The time delay between the two reflections, along with the linear frequency ramp of the source, gives rise to beat frequencies in the mixed output which are different for each cell. The connecting fiber length between two successive sensor cells is chosen to be much greater than the coherence length of the source so that the reflections from different cells do not interfere. The optical absorbance which is a characteristic of a chemical substance attenuates the amplitude of the optical signal passing the sensing cell [3], resulting in a decrease of the power spectrum amplitude for a given measurement point. The interference patterns of all sensor cells add up at the detector whereby each individual sensing cell is identified by its power spectrum in the frequency domain. We report theoretically and experimentally how individual cells can be addressed and the measured signals obtained by suitable choice of cell length, modulation of the source and appropriate signal processing. To demonstrate the feasibility of the proposed technique a system composed of three microoptic sensing units has been evaluated.

II. Microoptic Sensing Cell

The fiber microoptic sensing cell is constructed using two capillaries, two collimating GRIN lenses and a supporting V-groove alignment block. On both ends of the microoptic cell the capillaries are used to fix the fiber and align it to the center of the adjacent GRIN lens. As shown in Fig. 1 the capillary and GRIN lens are carefully aligned to minimize the air gap between them. Because the air gap could cause spurious backreflections, the gap is usually filled with index matching oil or gel.

For the proposed sensor systems the collimating GRIN lenses are turned with their antireflection coating facing the capillary. Therefore the main signal is partially reflected from the first lens, passes through the cell and is then partially reflected from the second lens. This reflected signal passes the cell once again and is coupled into the input fiber. The cell length is typically from a few millimeters up to several centimeters which is less

Manuscript received May 21, 1999; revised September 27, 1999.

M. Završnik is with the Faculty of Electrical Engineering and Computer Science, University of Maribor, Maribor 2000, Slovenia.

G. Stewart is with the Department of Electronic and Electrical Engineering, University of Strathclyde, Glasgow G1 1XW, U.K.

Publisher Item Identifier S 0733-8724(00)00391-1.

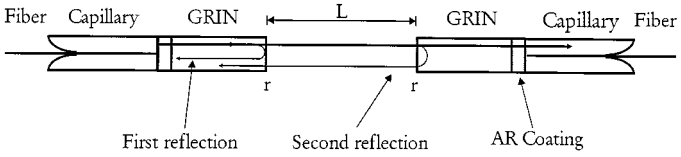

Fig. 1. Structure of the microoptic sensing cell.

than the coherence length of the laser source used. Typical values for surface reflectivities, $r_1^2 = r_2^2$, are 4%.

III. Mathematical Modeling and Simulation

The use of frequency modulation of a semiconductor laser is an attractive concept because of its simplicity and the high average power due to continuos-wave (CW) operation. The basis of coherent FMCW reflectometry is the interferometric mixing of two signals originating from the same linearly chirped source [4]. The frequency output of the laser diode is varied in a linear fashion, by driving the laser diode with a linear current ramp. Any time delays between the signals reflected back from the two interfaces give rise to beat frequencies in the mixed output. The configuration of the sensing array is shown in Fig. 2.

Here t_{ij} and r_{ij} represent the transmission and reflection coefficients at the interfaces for individual cells. The connecting fibers between two successive sensing cells are always much greater than the coherence length of the source, so signals from two different cells can not interfere.The system is essentially insensitive to the polarization state because, apart from the cell length, both reflected beams from each cell travel the same path and experience the same perturbations.

A. Signal Output

The absorption of light of incident intensity I_0 by a concentration, C, of a chemical or gas is described by the Beer–Lambert law

$$I = I_0 e^{-\alpha_m LC} = I_0 e^{-2\alpha_i LC} \tag{1}$$

where α_i is the amplitude attenuation coefficient and L is the cell length.

For the first sensing unit the optical field of both reflections returning along the fiber is given by

$$A^1_{\text{out}}(t) = r_{11}\sqrt{(A+Bt)}e^{j\omega t} + r_{21}t_{11}t'_{11} \cdot e^{-2\alpha_1 C_1 2L_1}\sqrt{(A+B(t-\tau))}e^{j\omega t+\psi+\Delta\psi)} \tag{2}$$

where

ω	angular frequency;
ψ	phase shift superimposed due to the time delay;
r_{11}, r_{21}	reflection coefficient;
t_{11}, t'_{11}	transmission coefficient in each direction at the glass/air interface.

The imposition of a dynamic shift in the frequency of the laser light $\Delta\omega$, due to the driving of the laser with a current ramp results in a dynamic shift of the phase ψ. ψ increases from a value $2\pi[2n_eL_1/\lambda_0]$ by a factor $\Delta\psi$ which equals $2\pi[2n_eL_1]\Delta\lambda//\lambda_0^2$ where L_1 is the length of the first sensing cell and $\Delta\lambda$ is the wavelength change due to modulation. A and B are constants and Bt represents the change in output light amplitude due to current ramping. We assume that the amplitude changes are small, therefore $B(t-\tau) \approx B(t)$.

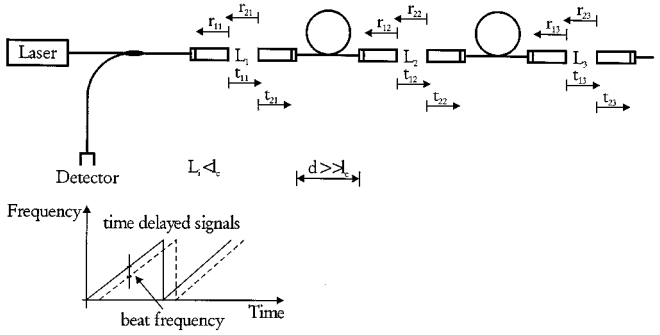

Fig. 2. FMCW with coherence addressing.

The output light intensity $I_{\text{out\_1}}$ for the first sensing cell is calculated by taking the first-order correlation of the total optical field $A^1_{\text{out}}(t)$, where the time variable is limited to one pulse of the beat frequency

$$\begin{aligned} I_{\text{out\_1}} \propto \langle A^1_{\text{out}} \cdot A^{1\,*}_{\text{out}} \rangle &= r_{11}^2(A+Bt) \\ &+ r_{21}^2 t_{11}^2 t_{11}'^2 (A+Bt)e^{-\alpha_1 C_1 4L_1} \\ &+ 2r_{11}r_{21}t_{11}t'_{11}(A+Bt)e^{-\alpha_1 C_1 2L_1} \\ &\cdot \cos\left(\frac{2\pi}{\lambda_0}\left(\frac{2n_eL_1}{\lambda_0}\right)(\lambda_0+\Delta\lambda)\right). \end{aligned} \tag{3}$$

The output light intensities for the second and third cell are calculated according to the first cell derivation. Additionally, we have to include absorption in the previous cells due to the serial arrangement of the system. The outputs read as

$$\begin{aligned} I_{\text{out\_2}} = {} & t_1^4 r_{12}^2 (A+Bt)\, e^{-\alpha_1 C_1 4L_1} \\ & + t_1^4 t_{12}^2 t_{12}'^2 r_{22}^2 (A+Bt) e^{-[\alpha_1 C_1 4L_1 + \alpha_2 C_2 4L_2]} \\ & + 2t_1^4 t_{12} t'_{12} r_{12} r_{22} (A+Bt) e^{-[\alpha_1 C_1 4L_1 + \alpha_2 C_2 2L_2]} \\ & \cdot \cos\left(\frac{2\pi}{\lambda_0}\left(\frac{2n_eL_2}{\lambda_0}\right)(\lambda_0+\Delta\lambda)\right) \end{aligned} \tag{4}$$

$$\begin{aligned} I_{\text{out\_3}} = {} & t_1^4 t_2^4 r_{13}^2 (A+Bt) e^{-[\alpha_1 C_1 4L_1 + \alpha_2 C_2 4L_2]} \\ & + t_1^4 t_2^4 t_{13}^2 t_{13}'^2 r_{23}^2 (A+Bt) \\ & \cdot e^{-[\alpha_1 C_1 4L_1 + \alpha_2 C_2 4L_2 + \alpha_3 C_3 4L_3]} \\ & + 2t_1^4 t_2^4 t_{13} t'_{13} r_{13} r_{23} (A+Bt) \\ & \cdot e^{-[\alpha_1 C_1 4L_1 + \alpha_2 C_2 4L_2 + \alpha_3 C_3 2L_3]} \\ & \cdot \cos\left(\frac{2\pi}{\lambda_0}\left(\frac{2n_eL_3}{\lambda_0}\right)(\lambda_0+\Delta\lambda)\right). \end{aligned} \tag{5}$$

The resultant interferometric signals add up at the detector and the power on the detector is a sum of individual unit outputs

$$I_{\text{out}} = I_{\text{out\_1}} + I_{\text{out\_2}} + \cdots + I_{\text{out\_}n}. \tag{6}$$

Here L_j is the length of the jth sensing cell and α_j the jth amplitude attenuation coefficient. The quantity t_1^2 is given from $t_1^2 = [t_{11}t_{21}t'_{11}t'_{21}] = (1-r_{11}^2)(1-r_{21}^2)$ and is the (power) transmission factor of cell (1). Similarly for t_2^2. If the two interfaces in each cell are similar, then $r_{11} = -r_{21}$, etc. Fiber losses are assumed negligible.

As already noted, the laser wavelength is ramped according to $\lambda = \lambda_0 + \Delta\lambda_{\max}(t/T)$ and so $\Delta\lambda$ in the cosine terms in (3)–(5) can be written as $\Delta\lambda = (\lambda - \lambda_0) = \Delta\lambda_{\max}(t/T)$ where T is the period of the ramp. Hence we can plot intensity from (6) versus time as shown in Fig. 3(a), where $T = 0.05$ s. Also with this substitution, the cosine terms become $\cos(\omega_b t + \psi)$ where the beat frequency $\omega_b = (4\pi n_e L_i \Delta\lambda_{\max})/\lambda_0^2 T$.

Signals from different cells are separated by transforming the output signal into the frequency domain. The calculated power spectrum for three sensing cells is shown in Fig. 3(b). The value of the wavelength change is approximately $\Delta\lambda_{\max} = 0.7$ nm, $A = B = 1, L_1 = 48$ mm, $L_2 = 60$ mm, $L_3 = 72$ mm, $\alpha C = 0.000625$ cm^{-1}, $\lambda_0 = 1300$ nm and the reflection coefficients chosen so that $r_{11}^2 = r_{21}^2 = r_{22}^2 = \cdots = 0.04$.

Different power spectrum peaks represent the different sensing units, whereby the beat frequency is mostly determined by the sensing length of the cell, i.e., separation between the GRIN lenses. Change in amplitude of the spectral peaks corresponds to information about absorption within a cell. Because different peaks represent different sensing units we have to lock on to each peak separately to perform measurements.

In order to compare the simulations and experimental results, we simulated absorption by introducing losses into the cells in fixed steps of ~0.35 dB (8% reduction of intensity). This was conveniently done by inserting microscope slides between the GRIN lenses. The 8% reduction arises from the 4% Fresnel reflection losses at each surface of the slide, and these reflections were directed away from the primary beam. First the measurements for a single cell were obtained, whereby the absorption was increased in steps of 8% from 0 to 32%. The change in the power spectrum amplitude is shown in Fig. 4.

In the next set of simulations, the number of slides for a cell was changed between zero and four and the change in power spectrum amplitude for individual cells was measured. The results are presented in Fig. 5. For Fig. 5(a) the absorption in the first cell is kept fixed at 0, 8, 16, etc., within the shaded blocks, while the absorption in the last cell is increased from 0 to 32% across the width of each shaded block. In the second cell no absorption is introduced. In Fig. 5(b), the absorption in the second cell is kept constant while the first cell absorption is changed from 0 to 32%. Here no absorption is present in the last cell.

To extract signals for individual cells signal processing is necessary. First, the first cell is evaluated and then the process is continued toward the last cell, thereby taking into account all previously calculated results.

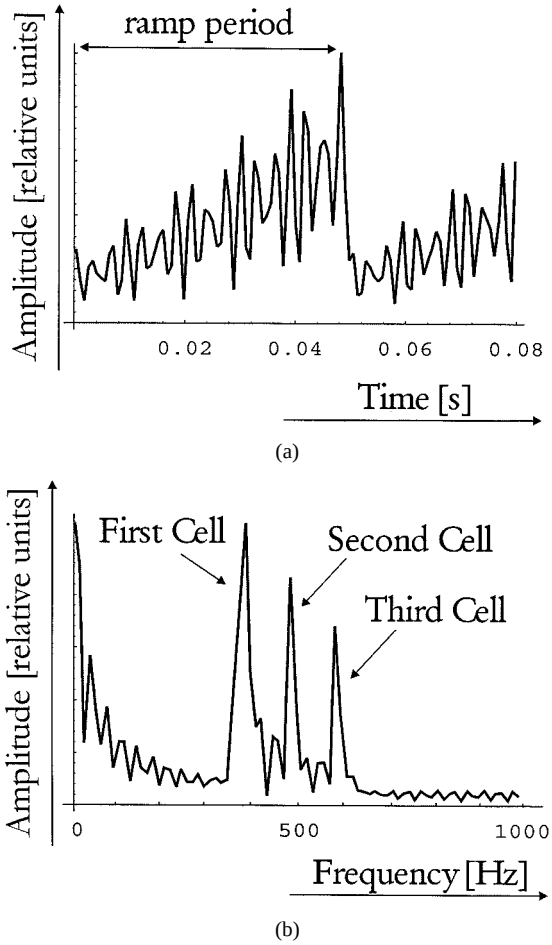

Fig. 3. (a) Time response during current ramp and (b) power spectrum for three cell FMCW with coherence addressing.

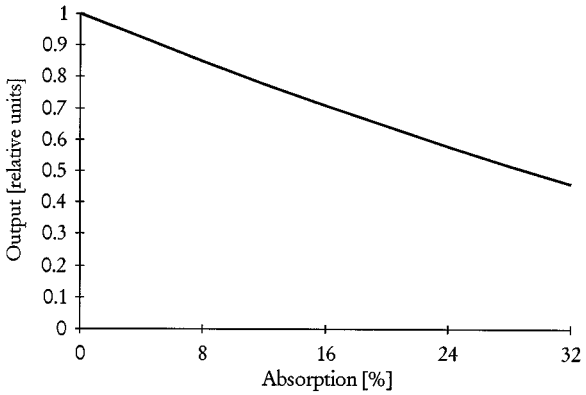

Fig. 4. Absorption for a single cell.

B. Limitation on Number of Cells in the System

When considering the coherence addressing of quasi-distributed absorption sensors by the FMCW method the maximum number of sensors is limited by two factors: the available space in the frequency domain and the signal to noise ratio (SNR).

The available space in the frequency domain is limited by the coherence length of the source. To distinguish between different beat frequencies in the power spectrum at the detector, every sensing unit should have its own unique optical path difference. With increase in coherence length of the source, the number of sensing cells each with a unique length can be increased. The maximum number of sensors $N_{\max f}$ due to the available frequency space is

$$N_{\max f} = \frac{\omega_c}{\Delta\omega} \tag{7}$$

where ω_c is the maximum beat frequency (with a source coherence length of 20 cm, $\omega_c \sim 1700$ Hz), and $\Delta\omega \sim 20$ Hz is the minimum resolvable difference between two beat frequencies. According to system parameters the maximum number of sensors due to the available frequency space is $N_{\max f} \sim 85$.

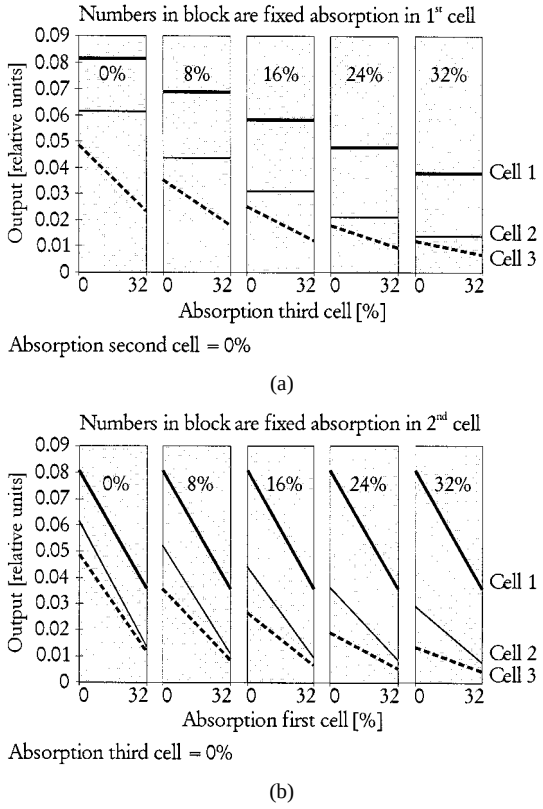

Fig. 5. (a) Absorption in the first cell held at fixed values shown and (b) absorption in the second cell held at fixed values shown.

The second limitation is the SNR, especially the SNR relating to the last cell in a chain of n cells. To calculate this ratio, we need to obtain the signal level from the last cell and also the receiver noise level. In general, the receiver noise consists of amplifier noise, dark current noise, shot noise and thermal noise. However, because our bandwidth requirements are very modest (5 kHz) and power levels on the detector are relatively high (up to milliwatt levels) a comparison of noise terms shows that shot noise limited detection is readily obtained.

We can compute the signal level as follows. From the third term of (3) the amplitude of the beat signal returned from cell 1 is approximately

$$I_{\text{beat\_1}} \approx 2r_{11}^2(1-r_{11}^2)(1-\alpha_{m1}C_1L_1)P_{\text{in}} \tag{8}$$

where P_{in} is the incident power. (Change in intensity due to current ramping has been neglected.)

The amplitude of the beat signal returned from cell n is reduced because the incident and returning beams have to pass through the preceding cells each with a transmission factor of t_i^2. Assuming that all cells have a similar throughput transmission of t^2 (~0.92) and a GRIN lens reflectance of r^2 (0.04) then

$$I_{\text{beat}\_n} \approx \left[(t^2)^{2(n-1)}\right] 2r^2(1-r^2)\left(1-\alpha_{mn}C_nL_n\right)P_{\text{in}}. \tag{9}$$

From (9) the reduction in the beat signal caused by absorption is

$$\Delta I_{\text{beat}\_n} \approx AP_{\text{in}}\left[(t^2)^{2(n-1)}\right] 2r^2(1-r^2) \tag{10}$$

where A is the absorbance ($A = \alpha_m CL$).

Assuming that the system is shot noise limited we can calculate the SNR for the absorption signal from cell n as

$$\text{SNR} = \frac{AP_{\text{in}}\left[(t^2)^{2(n-1)}\right] 2r^2(1-r^2)}{\sqrt{2e\Re P_{rec}B}} \tag{11}$$

where

- $\Re$ photodiode responsivity (~0.9A/W);
- B bandwidth (5 kHz);
- e electronic charge;
- P_{rec} total power received by photodiode.

In the worst case with a large number of sensors in the system, we assume that all the incident power is reflected back to the receiver and so, taking into account the 50 : 50 coupler, $P_{\text{rec}} \sim 0.5P_{\text{in}}$.

With these assumptions and substituting the values for the parameters, the worst case shot-noise-limited SNR is

$$\text{SNR} = [48.17 - 0.72(n-1) + 10\log A]\ dB. \tag{12}$$

Equation (12) predicts that we can still detect an absorbance of ~10^{-3} in the last cell at a SNR of ~5 dB, for the maximum cell number, $n = 20$.

From practical construction considerations, we do not anticipate to have more than ~20 cells in a system. The above results show that there should not be any problems in regard to either the available space in the frequency domain or in the signal-to-noise levels.

C. Analysis of Crosstalk

Although the selection of different optical path differences, i.e., cell lengths enables the separation between sensor signals in the frequency domain, it does not completely ensure their separation from "cross terms" which are the result of undesired interference between any two optical paths associated with more that one sensor in a system. If the cross terms are considered when designing the system, signals should be allocated in such a manner that cross terms do not coincide with any of the signals in the frequency domain.

Together with the interference from the sensing unit we get four additional interference terms resulting from the GRIN reflections in the neighboring sensing cells when crosstalk is considered. First is the interference between signals originating from the reflections on the first GRIN in the nth cell and the first GRIN lens of the $(n+1)$th cell. Second is the interference between reflections on the first GRIN in the nth cell and the second GRIN lens of the $(n+1)$th cell. The third is the interference between reflections on the second GRIN in the nth cell and the first GRIN lens of the $(n+1)$th cell, and the last is the interference from reflections on the second GRIN in the nth cell and the second GRIN lens of the $(n+1)$th cell.

Because of the crosstalk between sensing cells additional power spectrum peaks are visible (see Fig. 6). Their position along the frequency axis is dependent on the length of the cells used and the separation between them. For Fig. 6 reflectivities of the GRIN lenses were chosen as 0.04. The separation between the GRIN lenses of the nth and $(n+1)$th cells were chosen as 48 and 60 mm giving beat frequencies of 400 and

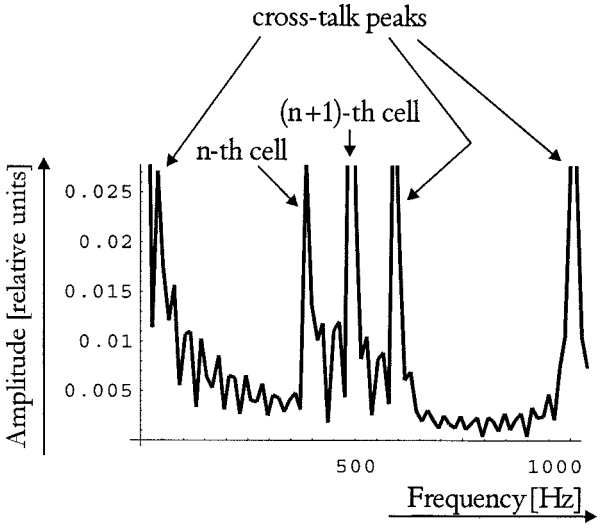

Fig. 6. Power spectrum for the coherence addressing scheme when crosstalk between sensing units is present.

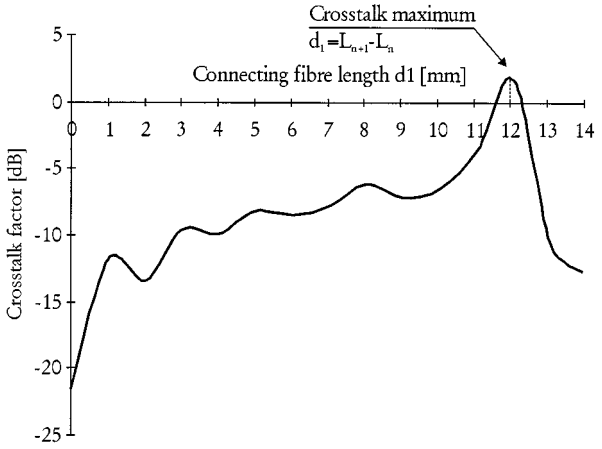

Fig. 7. The influence of the connecting fiber length on the crosstalk factor between adjacent cells for the coherence addressing of absorption sensors by the FMCW method.

500 Hz, respectively. A connecting fiber length of 12 mm was assumed between the cells.

A crosstalk beat frequency will coincide with the beat frequency of two adjacent cells if any one of the following conditions is satisfied

$$\begin{aligned} d_1 &= L_n \quad \text{or} \\ d_1 &= L_{n+1} \\ d_1 &= (L_{n+1} - L_n) \quad \text{or} \\ d_1 &= (L_n - L_{n+1}) \end{aligned} \tag{13}$$

where d_1 is the separation between the cells (the difference in index between cell and fiber is neglected here).

In principle, if crosstalk beat frequencies do not coincide with cell beat frequencies, then crosstalk is not a problem because measurements are taken by locking to cell beat frequencies, or the crosstalk frequencies may be eliminated by band pass filtering. In practice, however, because beat frequencies have a certain spectral width in the frequency domain (due to the finite time interval over which the signal is sampled by the spectrum analyzer), crosstalk will still influence measurements if crosstalk frequencies are sufficiently close to cell beat frequencies.

To analyze the effect we define the crosstalk factor for a cell as

$$CF = 10 \log \frac{CL - SL}{SL}. \tag{14}$$

Here SL is the power spectrum amplitude of the cell's beat frequency without crosstalk, and CL is the total (increased) amplitude, including crosstalk effects, also at the beat frequency for the cell.

Considering the same two adjacent cells as in Fig. 6 of lengths 48 and 60 mm, Fig. 7 shows the crosstalk factor for the 60 mm cell (at 500 Hz beat frequency) as a function of the connecting fiber length between the cells (spectrum analyzer sampling time interval of 10 μs). The figure shows clearly how the crosstalk grows as the connecting fiber length approaches 12 mm, at which point the crosstalk beat frequency is coincident with the cell beat frequency.

The simplest solution to avoid crosstalk between successive sensors is to make sensors incoherent with each other by introducing long time delays between sensors so that cross terms do not arise. If this is not possible then the following steps should be taken:

- the separation between successive cells should be different from any cell length;
- the sum of an arbitrary number of cell lengths should not match another cell length;
- the sum of an arbitrary number of cell lengths plus the fiber connection length should be different from any other cell length within the coherence length.

IV. Measurements

The feasibility of the proposed method was demonstrated by making the three-sensor system shown in Fig. 8. The optical source is a 1300-nm Nortel DFB laser diode. The output power is 1 mW with a coherence length of approximately 20 cm. The laser diode incorporated an internal optical isolator and thermoelectric heat pump for temperature stabilization. The output frequency of the laser diode was injection current modulated by a sawtooth waveform at a modulation frequency of 20 Hz and 10 mA current amplitude. The corresponding frequency excursion of the laser diode was approximately 90 GHz. The cells were constructed using GRIN lenses in V-grooves, with lengths $L_1 = 22$ mm, $L_2 = 33$ mm, $L_3 = 45$ mm.

In line with the simulations, first a single cell was evaluated and then three cells were placed in series and connected by a 20-m length of single-mode fiber. The individual power spectra where identified using a spectrum analyzer.

The time domain output signal for the three cell system which could be observed on the oscilloscope is shown in Fig. 9. The general shape of the time response is well predicted by (2) and corresponds to the theoretical calculations shown in Fig. 3(a).

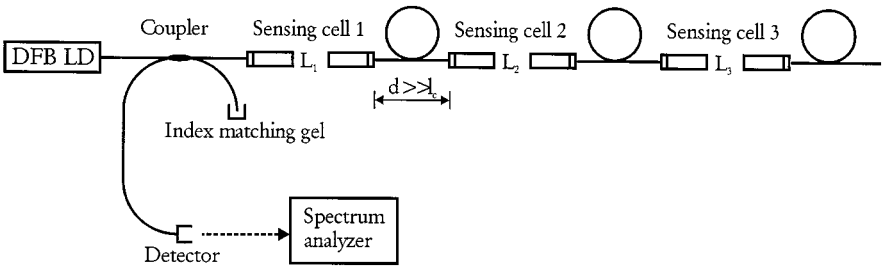

Fig. 8. Experimental setup for coherence addressing of quasidistributed absorption sensors by the FMCW method.

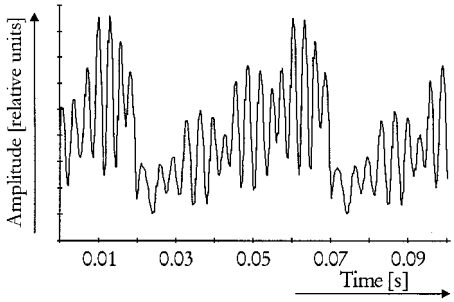

Fig. 9. Time response for the coherence addressed quasidistributed absorption sensors.

A. Experimental Power Spectrum

To evaluate the proposed system for absorption based measurements, the absorption inside individual cells was increased by inserting microscope slides between the GRIN's. Comparison between power spectra with and without absorption is presented in Fig. 10.

In Fig. 10(a) all three beat frequencies are clearly visible. After a microscope slide is inserted in the first cell the amplitude for all three power spectrum peaks is reduced in proportion to the absorption [Fig. 10(b)]. Similar the amplitude of the second and third beat peak is reduced after a slide is inserted in the second cell [Fig. 10(c)]. The final spectrum is obtained after one slide has been inserted in each cell. Also in Fig. 10(d), the difference between the power spectrum without, and with absorption present in each cell is indicated.

B. Absorption Measurement

Further investigations of the system were made by measuring the change in power spectrum amplitude for a particular beat frequency when absorption is increased. First a system with a single sensing unit has been evaluated. The experimental results (together with the computed results) are shown in Fig. 11, and, as expected, show the decrease in amplitude of the beat frequency in proportion to the absorption introduced.

Due to the successive arrangement of the sensing cells the influence from the cells in the beginning is transferred to subsequent cells. To analyze the influence of different levels of absorption for subsequent cells and the overall system performance a range of possible combinations of sensing cell absorption has been evaluated.

Fig. 12 shows the experimental results and the theoretical curves plotted in the same graph. In Fig. 12(a) the experimental and calculated results are in very good agreement and all three cells experience a small step change in attenuation as cell (1) attenuation is increased in fixed steps (from block to block) whereas only cell (3) experiences the attenuation of 0–32% across each block width.

This may be compared with Fig. 12(b) where all three cells experience the 0–32% variation in attenuation across each block introduced in cell (1), whereas only cells (2) and (3) experience the small step change from block to block introduced by the fixed attenuation changes in cell (2). Again, there is a good agreement between the computed and measured results.

Finally, Fig. 12(c) is similar to Fig. 12(b) except that cell (3) attenuation is increased in fixed steps from block to block instead of cell (2). Hence, only cell (3) experiences the slight decline from block to block as indicated by the dot-dash line.

Fig. 13(a) and (b) show in greater detail how the experimental output for the second and third cell, respectively, changes as the attenuation is varied in the cells indicated on the figure. Here also a comparison between computed and measured results is presented.

C. System Performance

For attenuation present at one cell only, the power spectrum amplitude at the cell's beat frequency was found to have a measurable range of 20 dB, i.e., a range of 20 dB on the vertical axis of Fig. 11. From Fig. 11, where the slope is ~2.5 dB signal per dB attenuation in the cell, a range of 20 dB on the vertical axis corresponds to a dynamic range of ~8 dB in attenuation measurement on the horizontal axis. However, due to the serial arrangement of the system, the available dynamic range of any individual cell is reduced when attenuation is present at earlier cells in the fiber line. For example if the first two cells have an attenuation present of ~0.3 dB, then the dynamic range of the third cell is reduced to ~6.8 dB.

For determination of system resolution, the noise level of the measurement was observed to be less then ~0.03 dB. Hence, a resolution of ~0.01 dB can be estimated.

In order to evaluate the response of the system to temperature change we heated the fiber at different locations (the lead in fiber before the coupler, after the coupler and the connecting fiber between the cells) using a laboratory gas burner. During the heating process the change in the power spectrum amplitude at the beat frequencies corresponding to individual sensing units were observed. We found that temperature change has a negligible influence on the system. Without regard to the location of the temperature influence, the power spectra changed less than the noise level.

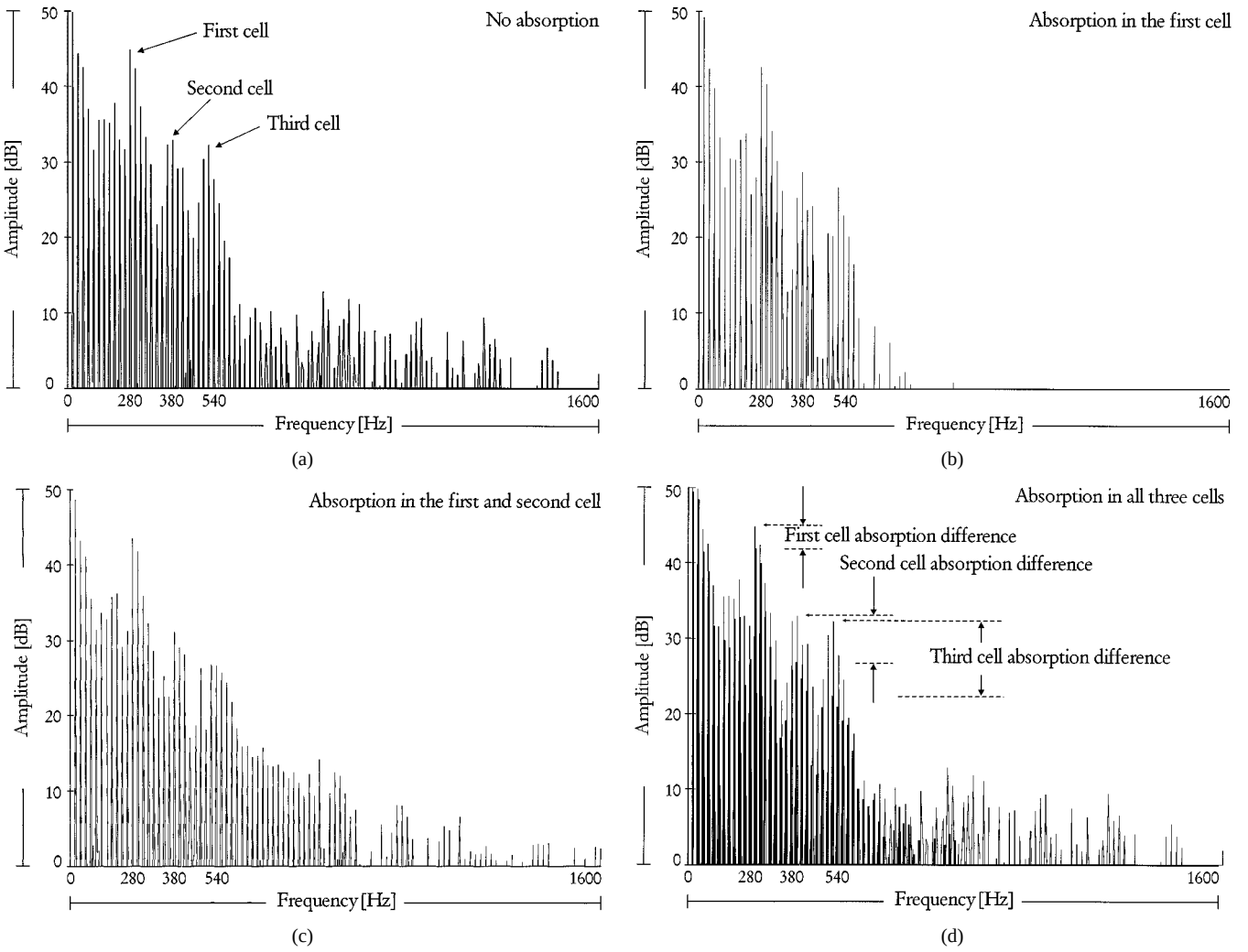

Fig. 10. Power spectrum of the FMCW Coherence addressed system: (a) without absorption, (b) microscope slide inserted in the first cell, (c) additional microscope slide inserted in the second cell, and (d) one microscope slide in each cell and comparison with the spectrum without absorption.

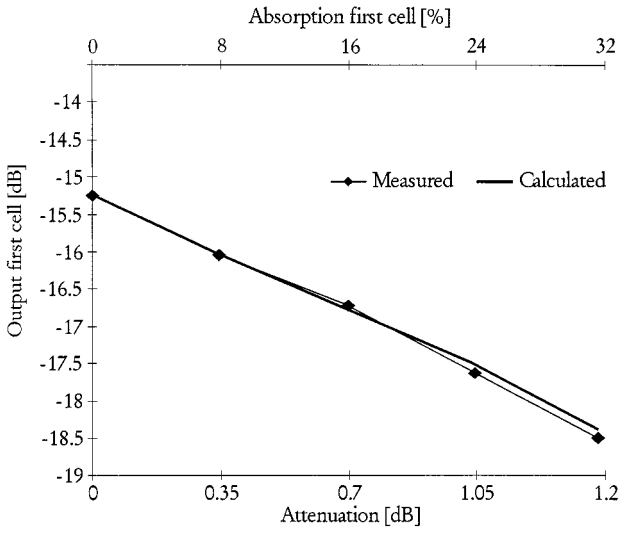

Fig. 11. Change in power spectrum amplitude for a single cell due to absorption.

The second disturbance which could influence the performance of the system are macro- and microbends of the lead in fiber, or the fiber which is connecting the sensing units. The system has been tested on macrobends by bending the fiber by hand and on microbends by pressing the fiber with a sharp object. Both bending mechanisms cause less than 0.05 dB change in the power spectrum amplitudes. The amplitude drop is mainly due to the microbend attenuation, since the macrobend effect is almost negligible. Basic precautions for avoiding or suppressing microbend effects is to use a fiber-optic cable designed to minimize microbend effects, and/or to shield the fiber from harsh mechanical influences.

Since a temperature controlled and current stabilized source is used, variations in source intensity are minimized, and in addition, a reference source power level can be extracted from the input coupler and used for feedback control of the source power.

D. Discussion

In general, the experimental and simulation results are in agreement. To take into account the mutual influence between cells due to the serial configuration, a calibration process at the beginning is necessary. Here, individual power spectrum peaks are identified and assigned to the sensing cells. When measurements are carried out, a power spectrum locking technique is used to collect the individual values. After all cells are scanned

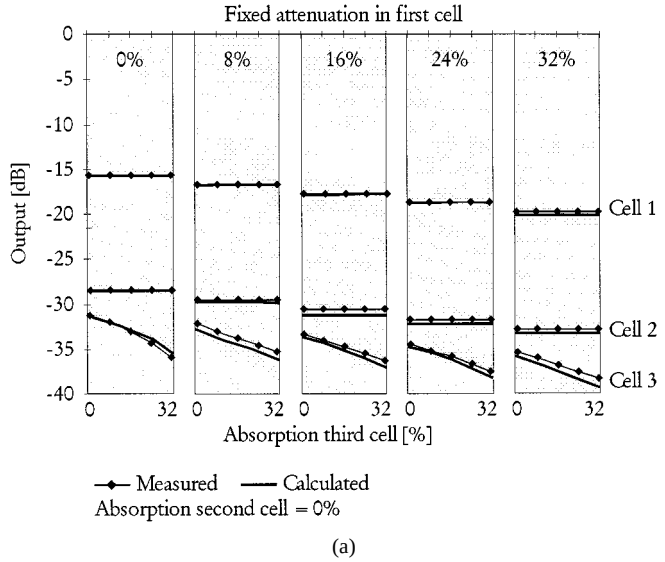

(a)

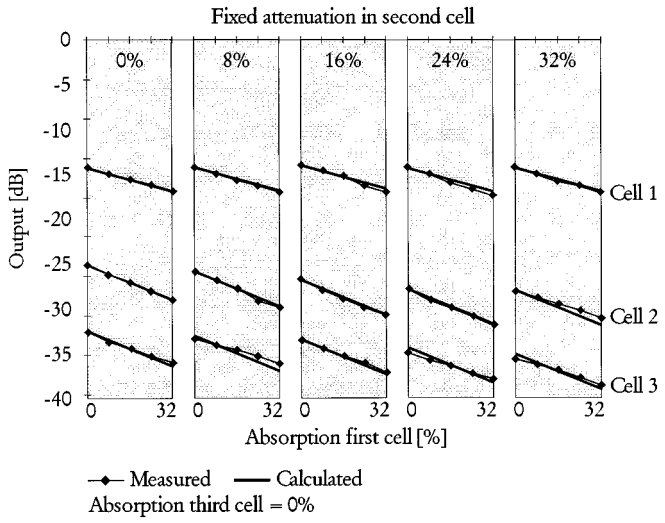

(b)

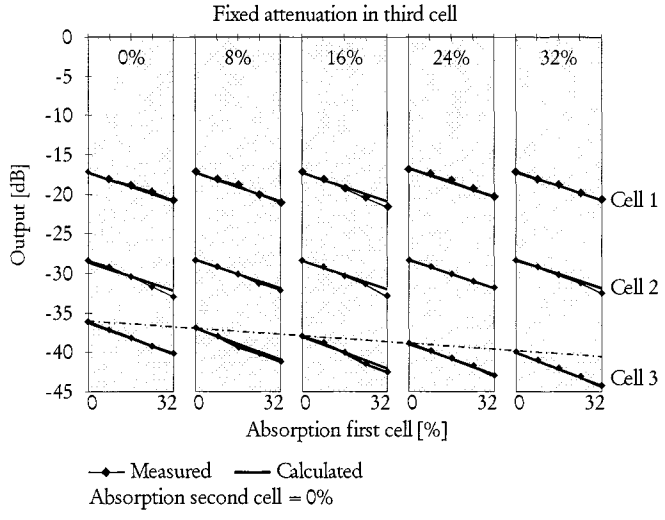

(c)

Fig. 12. (a) Absorption in the first cell held at fixed values shown. (b) Absorption in the second cell held at fixed values shown. (c) Absorption in the third cell held at fixed values shown.

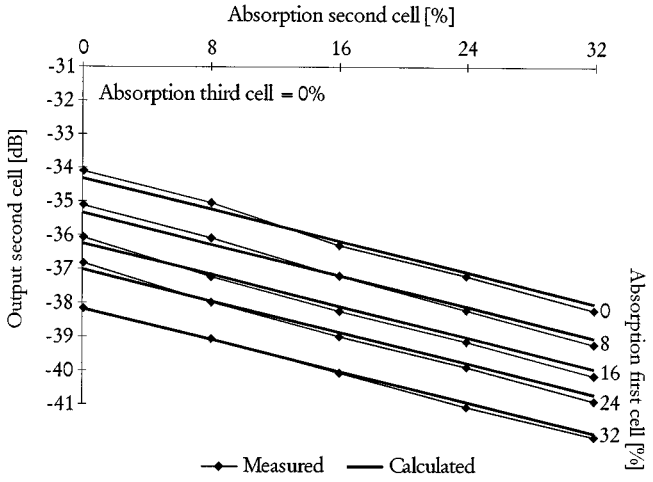

(a)

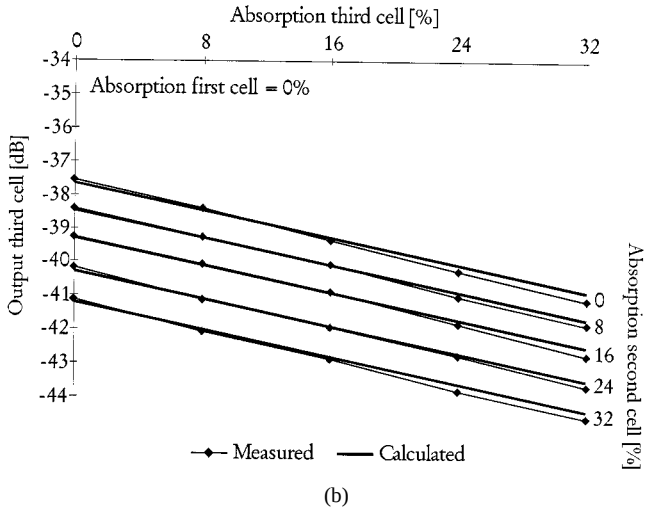

(b)

Fig. 13. (a) Output change for second cell due to absorption for different values of first cell absorption and (b) output change for third cell due to absorption for different values of second cell absorption.

the individual absorption value for each cell is calculated using previous calculations starting with the first cell.

One of the possible applications for the system is in measurement of gas concentration such as methane. The sensitivity level which is useful in practice (for methane alarm systems) is detection below the lower explosive level (LEL: 5% methane in air). For example, to detect 50% of the LEL and assuming a methane absorption coefficient[3] of $\alpha_m = 0.25\ \text{cm}^{-1}\text{atm}^{-1}$ for the (weak) near IR lines around 1665 nm, the system has to detect an attenuation of 0.27 dB or 6% change in the power spectrum amplitude for an individual sensing unit of length 5 cm. The experimental results presented (where the system has been evaluated using similar absorption values of ~8%, but with a broadband absorber) indicate that the proposed system is feasible for quasidistributed gas detection. However, because the methane gas absorption line-width is ~5 GHz then appropriate adjustment of the scan range and sweep time would be necessary. Although the current system has been evaluated using a scan range of 90 GHz, the scan range can easily be reduced to ~5 GHz while maintaining the same beat frequencies by reducing the sweep period from 0.05 s^{-3} ms. System operation using a narrow-band absorber is currently under investigation.

V. Conclusion

In this paper, a new approach for addressing quasidistributed interferometric absorbance sensors using coherence addressing and the FMCW method has been described. Coherence addressing of the cells using FMCW is achieved by the interferometric mixing of two signals originating from each cell. The optical absorbance, characteristic of a chemical absorber, attenuates the amplitude of the optical signal passing the sensing cell, resulting in a decrease of the power spectrum amplitude for a given measurement point. We have performed mathematical modeling with simulations and experimental verification of the proposed addressing mechanism and shown both theoretically and experimentally how different sensing cells can be addressed and how the information about the measurand can be acquired. Consideration of the available space in the frequency domain and the signal to noise ratio indicates that systems containing 20 serial sensing units are feasible. In order to take into account the mutual influence between cells due to the serial configuration, individual power spectrum peaks are identified and assigned to the sensing cells at the beginning of the measuring process. To avoid crosstalk between successive sensors it is desirable to make sensors incoherent with each other by introducing long connecting fiber lengths between sensing units, much greater then the coherence length of the source.

The feasibility of the proposed method was demonstrated using a three cell microoptic sensor system. One of the possible application areas for quasidistributed absorption based measurements is a distributed gas detection system, especially for methane. Here sensitivity levels below the lower explosive level of methane are readily achievable, enabling a serial arranged methane gas detection system.

References

[1] R. H. Wentworth, "Theoretical noise performance of coherence-multiplexed interferometric sensors," *J. Lightwave Technol.*, vol. 7, pp. 941–956, June 1989.

[2] D. Uttam and B. Culshaw, "Precision time domain reflectometry in optical fiber systems using a frequency modulated continuous wave ranging technique," *J. Lightwave Technol.*, vol. LT-3, pp. 971–977, Oct. 1985.

[3] G. Stewart, A. Mencaglia, W. Philip, and W. Jin, "Interferometric signals in fiber optic methane sensors with wavelength modulation of the DF laser source," *J. Lightwave Technol.*, vol. 16, pp. 43–53, Jan. 1998.

[4] S. Venkatesh and W. V. Sorin, "Phase noise considerations in coherent optical FMCW reflectometry," *J. Lightwave Technol.*, vol. 11, pp. 1694–1700, Oct. 1993.

[5] R. Passy, N. Gisin, J. P. von der Weid, and H. H. Gilgen, "Experimental and theoretical investigations of coherent OFDR with semiconductor laser sources," *J. Lightwave Technol.*, vol. 12, pp. 1622–1630, Sept. 1994.

Miha Završnik, photograph and biography not available at the time of publication.

George Stewart, photograph and biography not available at the time of publication.